International Journal of Concrete Structures and Materials

RESEARCH

Open Access

The Mechanical and Thermal Properties of Cement CAST Mortar/Graphene Oxide Composites Materials

Thidatip Janjaroen[1,2,3], Sunisar Khammahong[1,2,3], Wattana Tuichai[1,2,3], Attaphol Karaphun[1,2,3], Chaiwat Phrompet[1,2,3], Chaval Sriwong[1,3,4] and Chesta Ruttanapun[1,2,3*]

Abstract

This paper presents the influence of the graphene oxide (GO) sheet contents at conditions of 0, 0.01, 0.03, 0.05, and 0.1 wt% on the mechanical and thermal properties of GO/CAST 11 LW mortar (GMT) composites for heat insulating brick. The GMT composites were prepared by a simple mixing method. The structure of GMT composites was investigated by X-ray diffraction (XRD) and Raman spectroscopy (Raman) techniques. The small grain sizes of GMT composites were confirmed by transmission electron microscopy (TEM). The mechanical properties of GMT composites are increased with increasing GO contents. A lot of functional groups in GO such as carboxylic acid reacted with a calcium silicate hydrate, CaH_2O_4Si (CSH), calcium hydroxide, $Ca(OH)_2$ (CH) and Ettringite, and $Ca_6[Al(OH)_6]_2(SO_4)_3{\cdot}26H_2O$ (CA) phases in the mortar, which can be considered good mechanical properties in the GMT composites. The heat insulation values of GMT composites were improved by the interaction with the CSH, CH, and CA phases in the cement mortar on the surface of GO. The highest compressive and tensile strengths and low heat transfer rate of about 0.465 W/min were observed at 0.05 of GO (GMT_0.05) composites in the curing age of 7 days. Thus, a new pathway of GMT composites can be prepared by a simple mixing method to significantly improve the mechanical and thermal properties of mortar GMT composites.

Keywords: graphene oxide (GO) nanosheets, GO/mortar (GMT) composite, mechanical and thermal properties

1 Introduction

In recent years, the construction industry has tried to improve the properties of cement mortar using nanotechnology system composites (Naganathan et al., 2014; Raki et al., 2010; Sanchez & Sobolev, 2010). Although a high performance was observed in cement composites, the crack in structure was observed in those materials. The disadvantages of cement-based materials should be improved, e.g., being prone to cracking, low toughness, low tensile strength, and poor insulator (Dissanayake et al., 2017; Ferrándiz-Mas et al., 2014). A method to improve cement-based materials is to use composites with fillers which have excellent properties. Generally, the properties of cement composites are dependent on the fillers. For example, the thermal insulator properties of cement were reduced when the polyacrylamide (PAM) and fly ash cenospheres (FAC) fillers increased due to the low resistance of fillers (Kaya & Kar, 2016). Moreover, the high tensile strength and good stress properties were also improved by cement composites nanomaterial fillers (Cao et al., 2013; Jiang et al., 2018; Wang et al., 2021).

Over the last several years, the conventional nanomaterials including carbon-based nanomaterials such as carbon nanotubes (CNTs) (Li & Leung, 1992; Sagar et al., 2012), carbon black (Goracci & Dolado, 2020), carbon nanofibers (CNFs) (Popov, 2004; Roychand et al., 2016),

*Correspondence: chesta.ru@kmitl.ac.th; chesta.ruttanapun@gmail.com
[1] Smart Materials Research and Innovation Unit, Faculty of Science, King Mongkut's Institute of Technology Ladkrabang, Chalongkrung Road, Ladkrabang, Bangkok 10520, Thailand
Full list of author information is available at the end of the article
Journal information: ISSN 1976-0485 / eISSN2234-1315

MECNT (Lojka et al., 2021), Graphene Oxide (GO) (De Jong & Geus, 2000; De Volder et al., 2013; Llobet, 2013), and, reduced graphene oxide (rGO) (Geim & Novoselov, 2007; Wang et al., 2021; Zhou et al., 2016) have widely been used as fillers to improve the cement-based properties, including cracking, toughness, tensile strength, and thermal insulator. Less than 0.50 wt.% of the carbon nanomaterials were added to the cement-based materials to produce sustainable composites and to improve the mechanical properties and durability (Marcano et al., 2010; Zhu et al., 2010). GO is one of the good candidates because of its outstanding tensile strength, large surface area properties, and better dispersibility in aqueous media such as water (Compton & Nguyen, 2010; Gholampour et al., 2017). According to Wang et al. (2021) study, the effect of GO on the mechanical properties of cement composites is compared to rGOs. The tensile strength in GO–cement composites is higher than rGO–cement composites due to higher interactions of GO and CSH. Cao et al. (2013) reported that the increase in the tensile strength and compressive strength in 3 days to about 78.6 and 38.9% of cement–GO (0.03%) nanosheet composites was observed due to the formation of flower-like crystals. Namsone et al. (2017) reported that the specific mixtures of the GO solution and ordinary Portland cement with a curing age of 28 days showed maximum compressive strength at a GO content of 0.05 wt% and maximum tensile strength at a GO content of 0.03 wt%. The influence of GO composites on cement mortar composites was reported by Wang et al. (2017). The compressive strength was increased to 63% in 1% of nano GO–cement mortar composites in 28 days. Moreover, the compressive and tensile strengths of cement mortars GO composites at 0.03% of GO were observed at about 21.37 and 53.77%, respectively (Kang et al., 2017). According to Phrompet et al. (2019), the mechanical properties of cement-based composites were improved by the composites between rGO and man-sized C3AH6 cement. Although mechanical properties of cement composites are important in the infrastructure of buildings, the thermal insulation property is helpful in reducing the energy for cooling and heating in buildings (Du et al., 2020). Therefore, the GO has a good candidate material due to low thermal conductivity properties (Xu & Gao, 2011). Moreover, the improvement of the thermal insulation properties of cement-based composites by adding low GO concentrations has been rarely studied. The cements used in the study to fabricate cement composites were the cement CAST 11 LW mortar as insulating castable ASTM C 401 class 0. The chemical composition of cement was CaO (29.0%), Al_2O_3 (14.5%), SiO_2 (54.5%), Fe_2O_3 (0.5%) and SO_3 (0.5%). Therefore, in this work, the influence of the content of GO sheets on cement CAST 11 LW mortar composites in terms of compressive, tensile strengths and thermal properties was investigated for heat insulating castable brick at high temperature. The synthesized GO/CAST 11 LW mortar (GMT) composites with different contents of GO using the conditions of 0, 0.01, 0.03, 0.05, and 0.1 wt% were prepared and abbreviated as the GMT_0, GMT_0.01, GMT_0.03, GMT_0.05, and GMT_0.1 composites, respectively. The investigation of morphology and structure of (GMT) composites were observed by TEM, SEM, XRD, and Raman spectroscopy, respectively.

2 Experiments

2.1 Preparation of an Aqueous GO Suspension

GO suspension with a concentration of 2 mg/ml was prepared by a modified Hummers method, as previously reported in Phrompet et al. (2019) study. In brief, 2 g of graphite powder was mixed in a beaker with 6 g of $KMnO_4$ and poured into a 500-mL round-bottom flask at low temperature. Then, 46 mL of H_2SO_4 was gradually being added under stirring and cooling with maintained temperature below 15 °C for 15 min; and the temperature was increased to 40 °C for 30 min. After that, 90 mL of the distilled water was slowly added and heated up to 95 °C under stirring for 60 min. Consequently, the reaction of mixture was stopped by adding 10 mL of H_2O_2 solution and 250 mL of distilled water. Next, the obtained mixture was separated by the centrifugation and the sulphate was reduced by the wash with a 5% HCl solution. The mixture was washed and filtered several times using distilled water until the pH of filtered solution was about 7. Finally, supernatant of an aqueous GO suspension was obtained by ultrasonication of graphite oxide dispersed in deionized water (DI) and followed by centrifugation.

2.2 Preparation of Cement Composites

Firstly, an aqueous GO suspension was dispersed in the mixing DI water through ultrasonication process (at 250 Watt and frequency of 20 kHz) for 20 min using the mix composition, as listed in Table 1. The most widely applied method of improving the strength of cement is to uniformly disperse GO, which is soluble in water, and mix it with cement. Subsequently, a mortar (CAST 11 LW) cement was added into the GO water solution which was prepared at the ratio of 0.5 wt% using mixer at the speed of 218 rpm for 10 min. Then, the GMT composites were placed inside the mold and compacted for about 20 s to form specimens of the size of a cube of $50 \times 50 \times 50$ mm in dimensions for compressive strength and direct tensile using a Briquette mold. Then, all samples were kept in their molds at 100% relative humidity for 24 h. Before characterization, the GMT_0, GMT_0.01, GMT_0.03, GMT_0.05, and GMT_0.1 composites were cured under

Table 1 The mix design of the GMT composites, density of oven dry and saturated water, and % porosity.

Name	Mix proportion				Oven dry density (kg/m^3)	Saturated water density (kg/m^3)	Porosity (%)
	Cement (g)	Water (ml)	Aqueous GO suspension at concentrations (2 mg/ml)	W/C ratio			
GMT_0	1100	550	0	0.5	0.944 ± 0.008	1.252 ± 0.044	32.63
GMT_0.01	1099.945	522.5	0.055 g (27.5 ml)	0.5	1.012 ± 0.020	1.336 ± 0.056	32.02
GMT_0.03	1099.835	467.5	0.165 g (82.5 ml)	0.5	1.040 ± 0.032	1.336 ± 0.104	28.46
GMT_0.05	1099.725	412.5	0.275 g (137.5 ml)	0.5	1.056 ± 0.024	1.340 ± 0.076	26.89
GMT_0.1	1099.450	275	0.550 g (275 ml)	0.5	1.060 ± 0.036	1.280 ± 0.040	20.75

tap water for 3, 7, 21, 28 and 77 days at room temperature, as shown in Fig. 1a.

The crystal structure and characteristics of GMT composites were investigated by XRD (SHIMADZU/Japan, XRD-6100) and Raman spectroscopy (Thermo Fisher Scientific, DXR SmartRaman). The surface morphologies of GMT were observed by using TEM and SEM. The thermal analyzer of GMT composites was characterized by thermogravimetric analyzer (TGA, Perkin Elmer, Pyris 1). The thermal property was measured by using an Applied precision, ISOMET 2114. The thermal conductivity (κ) value was calculated via $\kappa = aDCv$, where a is the thermal diffusivity; D is the density of the sample; and Cv is the volumetric specific heat of the sample. The compressive strength of GMT composites was performed after 3, 7, 21, 28 and 77 days. The direct tensile strength of GMT composites was analyzed after 3, 7, 21, 28 and 77 days. Three specimens at each age were tested and the average compressive strength and tensile strength were calculated. The heat insulators of GMT composites were evaluated by using the multimeter (KEYSIGHT Technologies, U1241 C/U1242C 4-Digital Handheld). The infrared thermal imaging camera (Keysight Technologies U5856A, Range: − 20 to 650 °C) was used to observe the surface temperature distribution. The surface temperature was measured by using the multimeter with the type k probe measuring high and low temperatures, as shown in Fig. 1b. The temperature data were recorded by Keysight Handheld Meter Logger Software program for 7 h. Fig. 1c shows the samples of GMT composites.

3 Results and Discussion

The morphology and structure of GO sheets, GMT_0 and GMT_0.05 composite, were analyzed by TEM images as shown in Fig. 2a–c. Fig. 2a reveals the close-fitting presence of a large thin plate-like shape of GO sheets with translucent and crease surface as seen in the inset of Fig. 2a-1. Moreover, the SAED pattern in the inset of Fig. 2a-2 indicates the halo diffraction rings, signifying the amorphous layer with random orientations of a polycrystalline structure (Compton & Nguyen, 2010). Furthermore, the TEM images of GMT_0 and GMT_0.05 composites, as shown in Fig. 2b–c, respectively, discloses the fractions of particles with tiny particles of irregular shapes and micrometers in sizes of CSH phase in the cement mortar. The small incomplete grain growth of CH phase and the CA tube was found on CSH surface. The CA tube appeared as rod-like crystals in the early stages of reaction as massive growths filling pores or cracks in mature concrete or mortar. It can be seen in the high-magnification image of Fig. 2c-1 that the surface of CSH phases is seized by GO sheets which increases the tightness of both the hardened cement paste and mortar. The SAED pattern in the inset of Fig. 2b-2 displays the diffraction spots of GMT_0 sample, while GMT_0.05 composite reveals the concentric diffraction rings of spots as shown in inset of Fig. 2c-2, indicating a polycrystalline nature (Liu et al., 2014). This result confirms the existence of GO sheets embedded in the GMT_0.05 composite. Fig. 2c-3 indicates the EDS spectra of GMT_0.05 composite which has the C, Al, Ca, Si, and O elements (Liu et al., 2014).

Fig. 3a shows XRD pattern of GO sheets, GMT_0, GMT_0.01, GMT_0.03, GMT_0.05, and GMT_0.1 composites, respectively. The XRD pattern of GO sheets displays a broad diffraction peak appeared at 2° of 11.16° which corresponded to the crystalline planes of (002) with a determined d-spacing of 0.810 nm (Phrompet et al., 2019). Next, XRD pattern of GMT_0, GMT_0.01, GMT_0.03, GMT_0.05, and GMT_0.1 composites can detect the phases of the usual cement hydrates as calcium silicate hydrate (CaH_2O_4Si; CSH), calcium hydroxide ($Ca(OH)_2$; CH) and Ettringite ($(Ca_6[Al(OH)_6]_2(SO_4)_3{\cdot}26H_2O$; CA) and silicon dioxide (SiO_2; Si) (Wang et al., 2017). The XRD results can confirm the pure phase of cement mortar.

The Raman spectra of GO sheets, GMT_0, GMT_0.01, GMT_0.03, GMT_0.05, and GMT_0.1 composites are shown in Fig. 3b. Generally, the

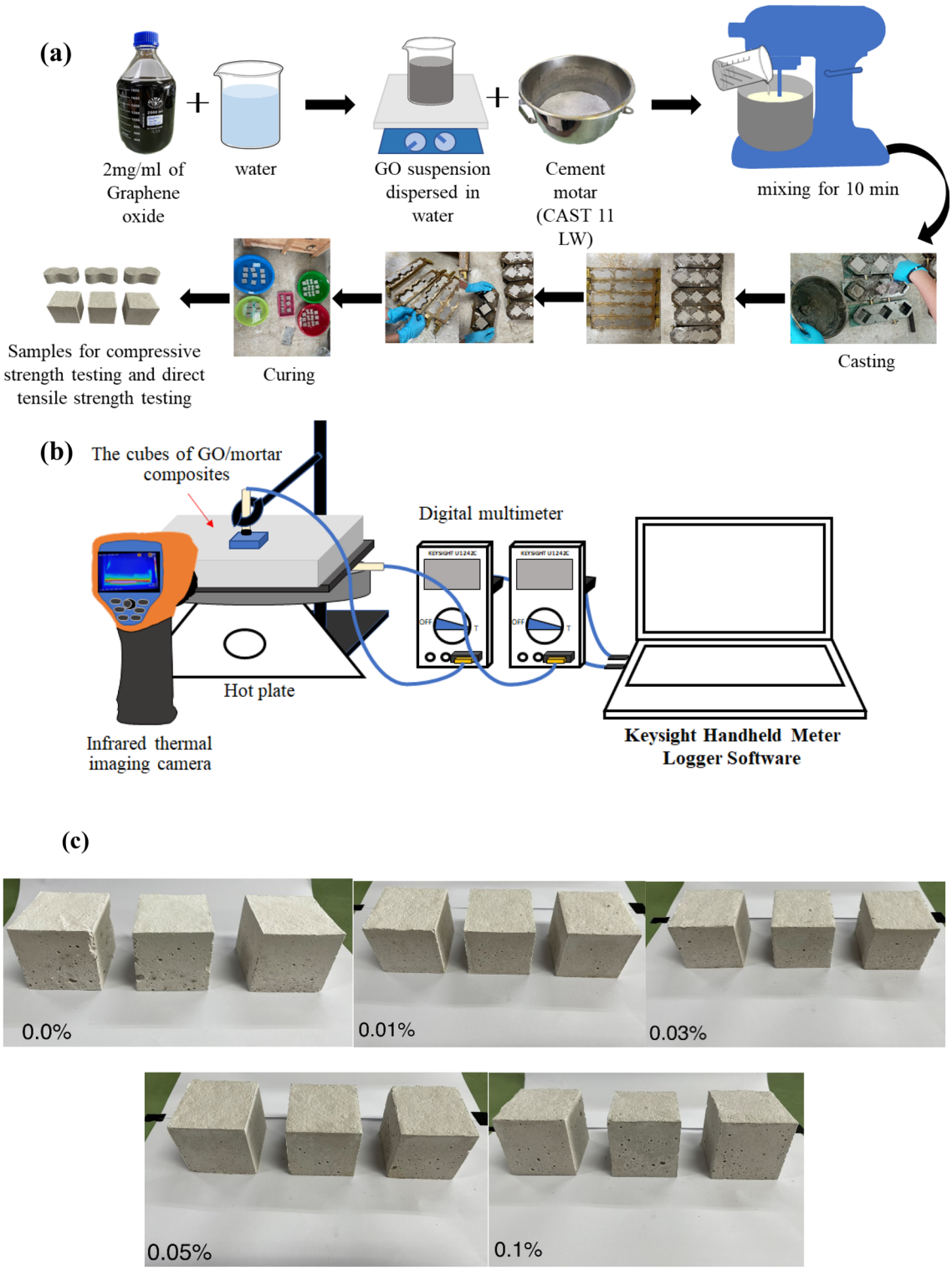

Fig. 1 a The preparation of the cubes of GMT composites, b the experimental prosecution for the measurement of the temperature difference between the hot and cold at surfaces of GMT composites, and c the photographs of GMT composite samples.

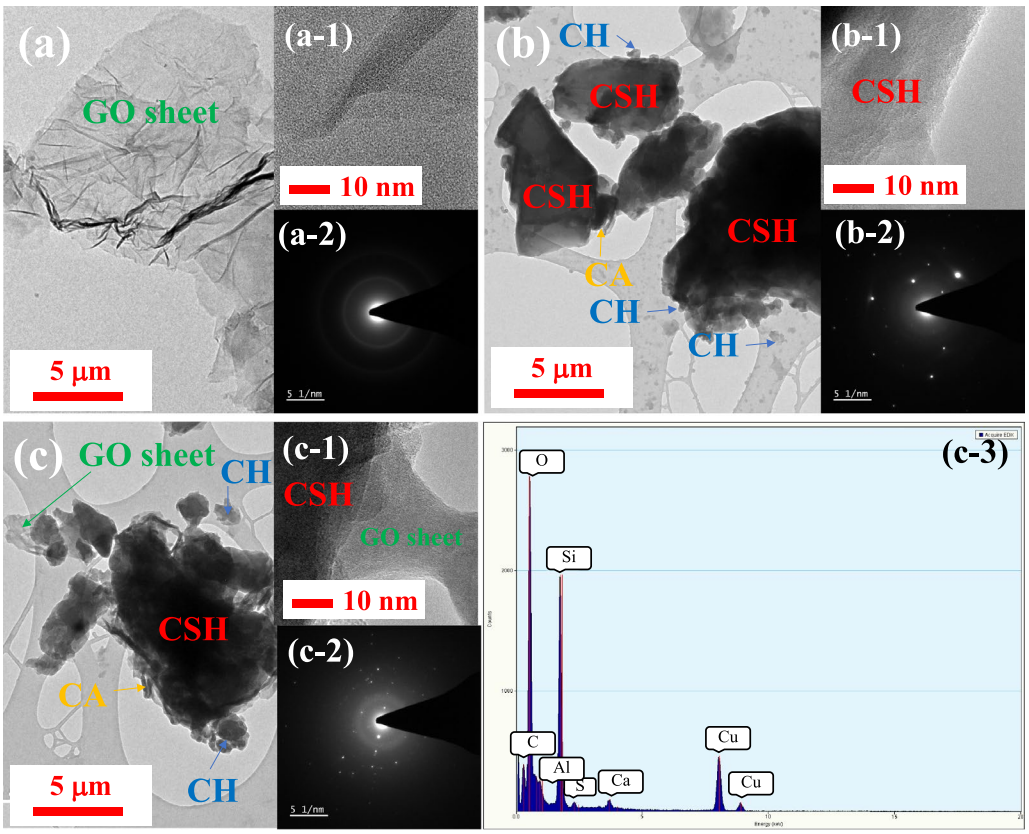

Fig. 2 TEM image, the high-magnification image and SAED patterns of a GO sheets, b GMT_0 and c GMT_0.05 composite which has the energy dispersive X-ray (EDX) spectra of GMT_0.05 composite.

Raman spectra of GO sheets displays two main peaks at ~ 1338 cm^{-1} and ~ 1586 cm^{-1}, known to be the D and G-bands in the structure of carbon atom, respectively (Phrompet et al., 2019; Suk et al., 2010). In principle, the D-band defects and disorders the first hexagonal graphitic layers. In addition, the G-band is related to the sp^2-bonded carbon atom vibration in 2D hexagonal lattice (Phrompet et al., 2019; Suk et al., 2010). Next, Raman spectra of GMT_0, GMT_0.01, GMT_0.03, GMT_0.05, and GMT_0.1 composites are observed as well as pure mortar (Carrasco et al., 2017). The band at ~ 714 cm^{-1} is determined by asymmetric stretching of Si–O–Al and the band at 1088 cm^{-1} may be attributed to lattice mode. Next, the bands at ~ 953 cm^{-1} are assigned to $\upsilon_1(SiO_4)$ symmetric stretching vibration of C–H–S phase, which is the main phase formed during cement hydration (Carrasco et al., 2017). The band at ~ 670 cm^{-1} is determined by asymmetric stretching of Si–O–Si bending modes involving tetrahedra. The bands at ~ 483 cm^{-1} are symmetric bending υ_2(Si–O) and small band at ~ 365 cm^{-1} is ascribed to residual $Ca(OH)_2$ (Carrasco et al., 2017; Suk et al., 2010). The band at ~ 299 cm^{-1} is assigned to the deformation of the silicate network along with Ca–O stretching (Phrompet et al., 2019; Suk et al., 2010). These results indicated that all samples are at the pure phase of cement mortar. At high composite concentrations (> GMT_0.03), the two peaks were obviously observed indicating the influence of GO composites which increases the tightness of both the hardened cement paste and mortar.

TGA data are demonstrated in Fig. 3c. The weight loss and DTG peaks of GMT composites gradually decreased with increasing temperature. This result indicated a specific phase of compounds decomposition. The three steps of decomposition in all samples were observed. At a low temperature ~ 30–100 °C, the decreasing weight loss of about 4% should be related to the decomposition of the absorbed water molecules (Singh et al., 2015). At temperature ~ 100–500 °C, the decreasing weight loss should be the decomposition of CSH, mono-carbonate. Moreover, at the high temperature range of 600–750 °C, the major weight loss was observed because of the decomposition of the calcined as CO_2 (Singh et al., 2015). Interestingly, the DTG peak of GMT composites gradually increased when the concentrations of GO increased. This result indicated that the concentrations of GO can improve the

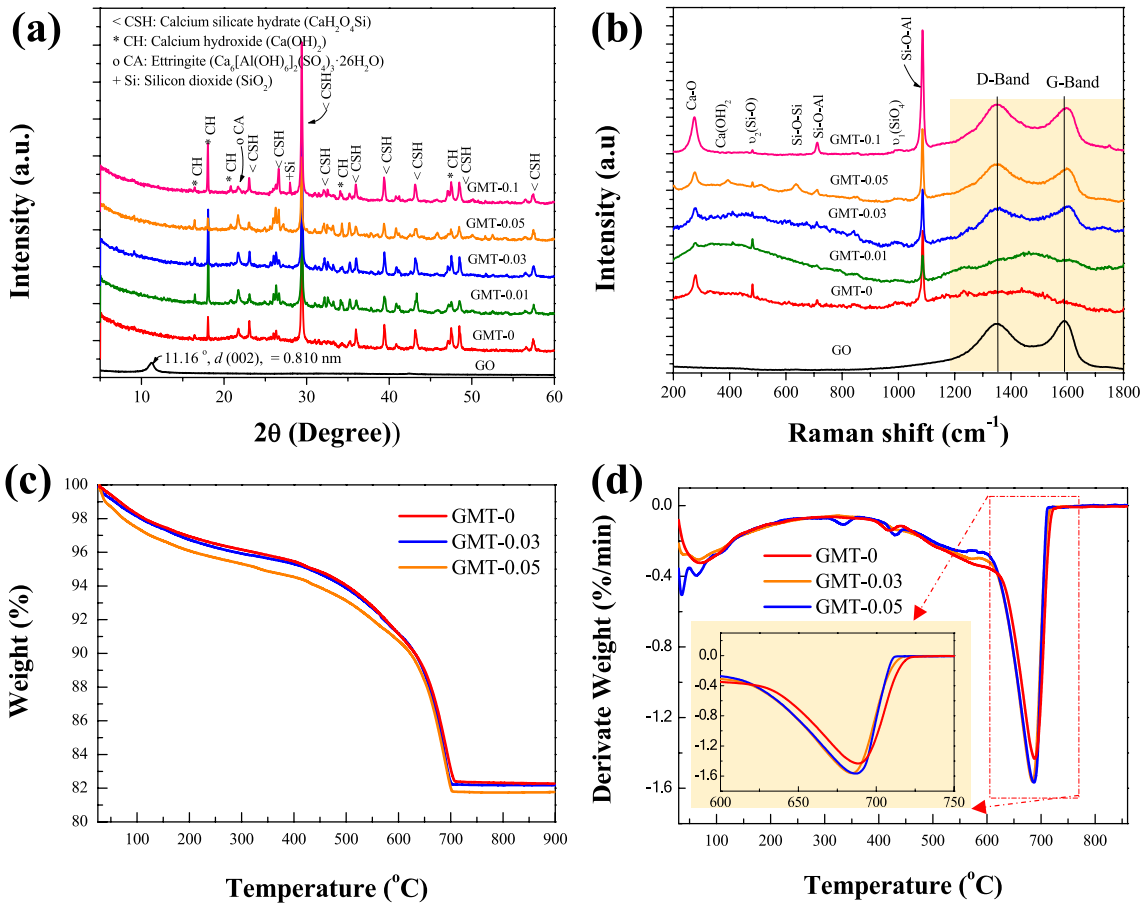

Fig. 3 a XRD patterns, b Raman spectra, c TGA curves, and d DTG curves of GO sheets, GMT_0, GMT_0.01, GMT_0.03, GMT_0.05, and GMT_0.1 composites, respectively.

thermal stability in mortar composites as shown in the inset of Fig. 3d.

The relationship between mechanical properties and the microstructure of the composites was characterized by SEM images. However, the GO sheets are not detected due to small sheets. The surface of the mortar particle should be deposited by the GO sheet. According to Fig. 4a–d, the SEM images of the GMT_0, GMT_0.03, GMT_0.05 and GMT_0.1 composites reveal random sizes and the content of CH, CA, and CSH as ordinary cement mortar. Obviously, the influence of GO on cement mortar size can improve the micro-compactness, micro-cracks and low percentage porosity (Lv et al., 2013), as shown in Table 1. Therefore, adding GO to low contents of GMT composites can increase the mechanical properties because the GO sheet plays the role of a bridge through covalent bonding with CSH (Kang et al., 2017).

Fig. 5a shows the comparison of compressive strengths at the curing age of 3, 7, 21, 28 and 77 days for GMT_0, GMT_0.01, GMT_0.03, GMT_0.05, and GMT_0.1 composites, respectively. The compressive strengths of the GMT_0.01, GMT_0.03, GMT_0.05, and GMT_0.1 composites were greater than GMT_0 (without GO loading) sample for all the curing ages at 3, 7, 21, 28 and 77 days, respectively, as summarized in Table 2. The excellent mechanical properties of GMT composites compared with GMT_0 explained by a lot of functional groups in GO, such as carboxylic acid that reacted with CSH, CH and CA in the mortar, should be forming a strong covalent bond (Qureshi & Panesar, 2019). A curing age at 7 days had the highest percentage compressive strength value of 11.084 ± 0.620 MPa when the GO content was 0.05 wt% (GMT_0.05) which is higher than the percentage value of GMT_0 approximately 36.71%, as shown in Fig. 5b. Namsone et al. (2017) reported that the 28-day compressive strengths were observed about 6.68–12.49 MPa for a foamed matrix using expanded glass aggregates in cement mortar. Moreover, Rafiee et al. (2013) reported that the compressive strength of

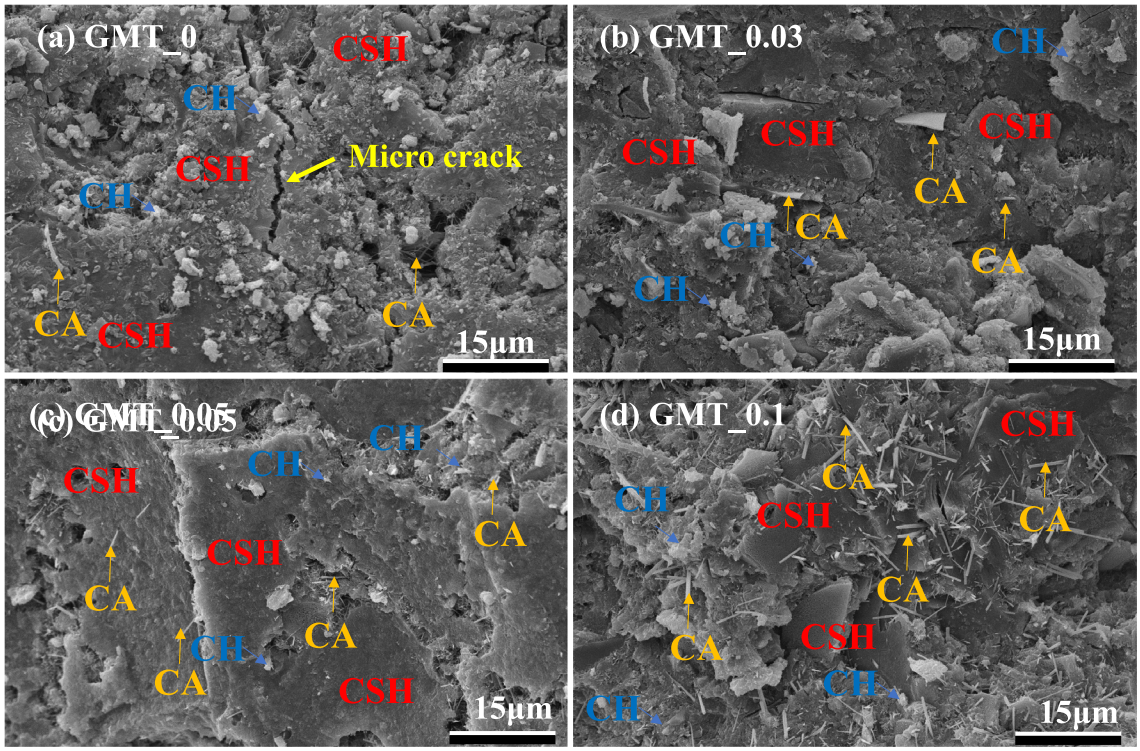

Fig. 4 SEM images of GMT_0, GMT_0.03, GMT_0.05 and GMT_0.1 composites, respectively.

the mixture increased by approximately 15% in comparison to ordinary mortar when the GO concentration was 1.0 wt% as GO reinforces the crevices in cement. However, at the high GO concentrations > 0.05 wt%, the compressive strengths gradually decreased because of the self-accumulation of GO sheets. Furthermore, when the curing age under tap water is higher than 7 days, the percentage compressive strength showed a low value by approximately 26.83, 17.00, 32.71 and 34.70% for the curing age at 3, 21, 28 and 77 days, respectively, measured by a GMT_0.05 sample. Fig. 5c shows a comparison between the tensile strengths of GMT_0, GMT_0.01, GMT_0.03, GMT_0.05, and GMT_0.1 composites, respectively, at the curing age of 3, 7, 21, 28 and 77 days to analyze the effect of GO on tensile strength. The tensile strength of GMT_0.05 sample was demonstrated to be the highest by up to 61.45% at 7 days of a curing age as shown in Fig. 5d. As Qian et al. (2015) reported that the compressive strength of cement composite specimens with low GO concentrations of 0.05 wt% increased by up to and 18.7% and 13.7% at a curing age of 7 and 28 days, respectively. The tensile strength values of all sample are summarized in Table 2. The strengths of the GMT composites increased in the compressive and tensile strength tests because of the addition of GO which promotes hydration, decreases pore volume, accelerates crystallite formation, and causes the crystallites to align. This increases the tightness of both the hardened cement paste and mortar (Liu et al., 2012). Also, the mechanical property of cement mortar was improved by the GO composites.

Fig. 6a–b demonstrates the volumetric heat capacity (Cv), the thermal conductivity (κ), and thermal diffusivity (a) of GMT_0, GMT_0.01, GMT_0.03, GMT_0.05, and GMT_0.1 composites, respectively at the curing age of 7 days. In Fig. 6a, the volumetric heat capacity values were 1.489×10^6, 1.471×10^6, 1.449×10^6, 1.515×10^6 and 1.408×10^6 J/m^3 K for GMT_0, GMT_0.01, GMT_0.03, GMT_0.05, and GMT_0.1 composites, respectively.The results showed that the GMT_0.05 had the lowest Cv value compared to other samples. Furthermore, the thermal conductivity and the thermal diffusivity are shown in Fig. 6b. The thermal conductivity was found to be 0.578 ± 0.008, 0.568 ± 0.023, 0.549 ± 0.025, 0.513 ± 0.028 and 0.490 ± 0.026 W/m K for GMT_0, GMT_0.01, GMT_0.03, GMT_0.05, and GMT_0.1 composites, respectively, whereas the values of thermal diffusivity were found to be at the range of 0.38×10^{-6} to 0.33×10^{-6} m^2/s. The thermal conductivity value of mortar about 0.264 W/m K is similar to what was observed in Jiang et al. (2018) study. The thermal conductivity is decreased with increasing GO contents due to the low thermal

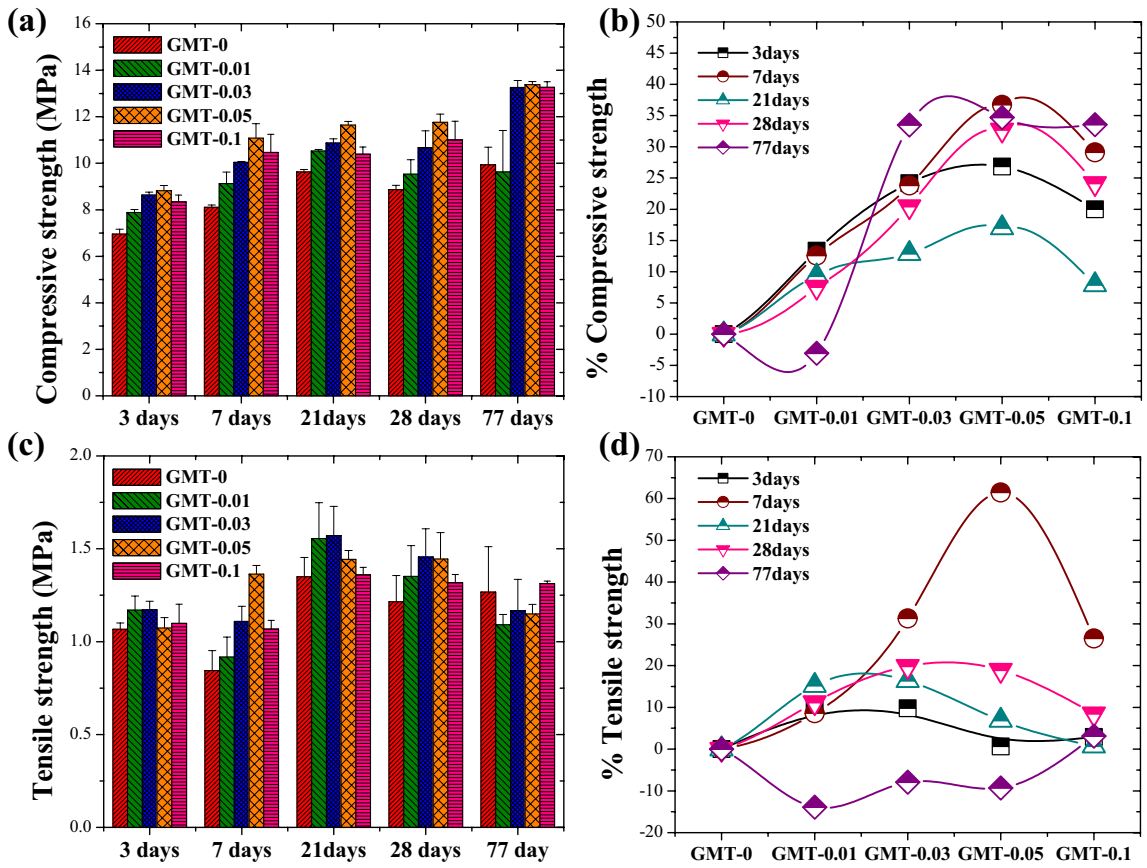

Fig. 5 The comparative graphs of a compressive strengths and b % compressive strengths, c tensile strength and % tensile strength at the curing age of 3, 7, 21, 28 and 77 days of GMT_0, GMT_0.01, GMT_0.03, GMT_0.05, and GMT_0.1 composites, respectively.

Table 2 Compressive strengths and tensile strength of GMT_0, GMT_0.01, GMT_0.03, GMT_0.05, and GMT_0.1 composites at the curing age of 3, 7, 21, 28 and 77 days, respectively.

The curing age	Samples				
	GMT_0	GMT_0.01	GMT_0.03	GMT_0.05	GMT_0.1
Compressive strengths (MPa)					
3 days	6.954 ± 0.212	7.882 ± 0.127	8.635 ± 0.122	8.819 ± 0.225	8.344 ± 0.292
7 days	8.107 ± 0.097	9.126 ± 0.496	10.037 ± 0.044	11.084 ± 0.620	10.467 ± 0.780
21 days	9.631 ± 0.099	10.524 ± 0.070	10.871 ± 0.178	11.641 ± 0.157	10.389 ± 0.311
28 days	8.864 ± 0.191	9.533 ± 0.618	10.676 ± 0.721	11.763 ± 0.352	11.004 ± 0.802
77 days	9.936 ± 0.756	9.631 ± 1.776	13.262 ± 0.299	13.282 ± 0.132	13.268 ± 0.235
Tensile strength (MPa)					
3 days	1.067 ± 0.033	1.169 ± 0.075	1.171 ± 0.045	1.073 ± 0.056	1.098 ± 0.103
7 days	0.844 ± 0.107	0.916 ± 0.107	1.108 ± 0.081	1.363 ± 0.046	1.068 ± 0.046
21 days	1.349 ± 0.103	1.555 ± 0.192	1.571 ± 0.157	1.442 ± 0.047	1.359 ± 0.040
28 days	1.215 ± 0.141	1.351 ± 0.166	1.456 ± 0.152	1.445 ± 0.142	1.318 ± 0.043
77 days	1.267 ± 0.244	1.091 ± 0.055	1.166 ± 0.168	0.149 ± 0.051	1.312 ± 0.015

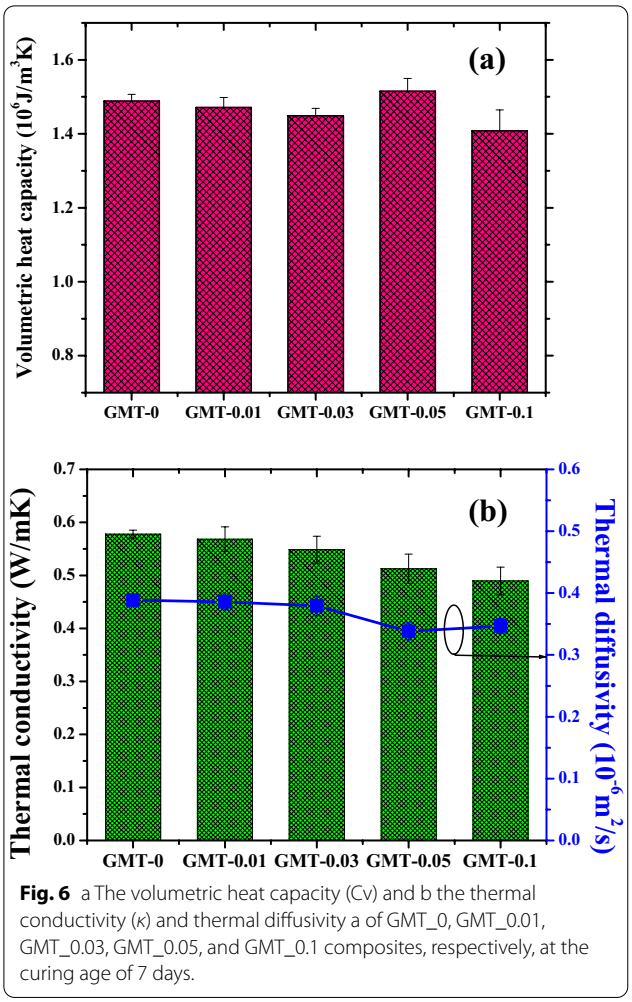

Fig. 6 a The volumetric heat capacity (Cv) and b the thermal conductivity (κ) and thermal diffusivity a of GMT_0, GMT_0.01, GMT_0.03, GMT_0.05, and GMT_0.1 composites, respectively, at the curing age of 7 days.

conductivity or the exellent insulator of GO sheets and good interactions between CSH, CH and CCA phases in the cement mortar and GO sheets. The low thermal conductivity was observed at 0.05 wt% (GMT_0.05) and 0.1 wt% (GMT_0.1) of GO content similar to what was observed in the low thermal insulation property of GMT composites. Generally, the material with thermal conductivity values lower than 0.250 W/m K is known as a heat insulator material (Zhou et al., 2010). Therefore, the heat insulator of cement mortar was enhanced by the GO composites.

The heat insulator behavior of GMT_0, GMT_0.01, GMT_0.03, GMT_0.05, and GMT_0.1 composites at the curing age of 7 days was investigated. The temperature distribution on the surface of GMT composites was observed at the experimantal time for 0, 10, 20 and 30 min by using the infrared thermal imaging as shown in Fig. 7. The temperature of the hot surface was 350 °C. According to Fig. 7, both sides of temperatures on high temperature and low temperature for all GMT composites are increased with increasing time until the temperature becomes constant. The results showed that all GMT composites displayed temperature stability on the hot plate at the same time about 30 min. The heat insulator behavior of mortar is similar to what was reported in another study conducted by Yousefi et al. (2020). In all GMT composites, the increase of low temperature was observed as well as pure mortar (GMT_0). The temperature differences (ΔT) of each surface side are particularly important because the materials, which can block the heat transfer, should be applied to insulating material between the hot and cold surface of thermoelectric devices. The insulating materials can increase the output efficiency in energy conversion devices such as thermoelectric devices. For example, Lv et al. (2020) reported that the output efficiency of thermoelectric device increased with the decrease of the thermal properties of fillers in space between legs. Moreover, the output efficiency of thermoelectric properties decreased about ~ 1% because the thermal insulation materials are not added in the space between legs according to Li et al. (2018). Therefore, the heat insulation materials should be a factor causing the increase in the output efficiency of thermoelectric properties because of the reduction or elimination of the heat transfer (Li et al., 2018; Lv et al., 2020). The ΔT values of GMT composites are summarized in Table 3 and found to be at the range of 276–279 °C and 269–271 °C for 20 and 30 min, respectively. Interestingly, for GMT_0.05 and 0.1 composites, the temperature difference values increased due to the low thermal conductivity of GO sheets compared with the rGO or Graphene (Mahanta & Abramson, 2012). Moreover, the reaction with CSH and CH phases in the cement mortar on the surface of GO should reduce the thermal insulation property of GMT composites.

Furthermore, the thermal resistance (R), which is the resistance to heat flow as heat insular of the material of GMT composites, was defined by $R = t/\kappa$, where t is the insulation thickness and κ is the thermal conductivity of sample (Mahanta & Abramson, 2012). The thermal resistance values of GMT composites in the area of 5×5 cm^2 and thickness of 5 cm are summarized in Table 3. The thermal resistance value was 0.087, 0.115, 0.091, 0.098 and 0.102 m^2 K/W for samples of the GMT_0, GMT_0.01, GMT_0.03, GMT_0.05, and GMT_0.1 composites, respectively. The sample of GMT_0.05 and GMT_0.1 composites displayed the high thermal resistance value. This result indicated that those samples provided the high thermal resistance values.

The investigation of the surface by overall heat transfer coefficient (U) as inversion of thermal resistance value was done through $U = 1/R$ (Mahanta & Abramson, 2012; Zhou et al., 2010). The overall heat transfer coefficient

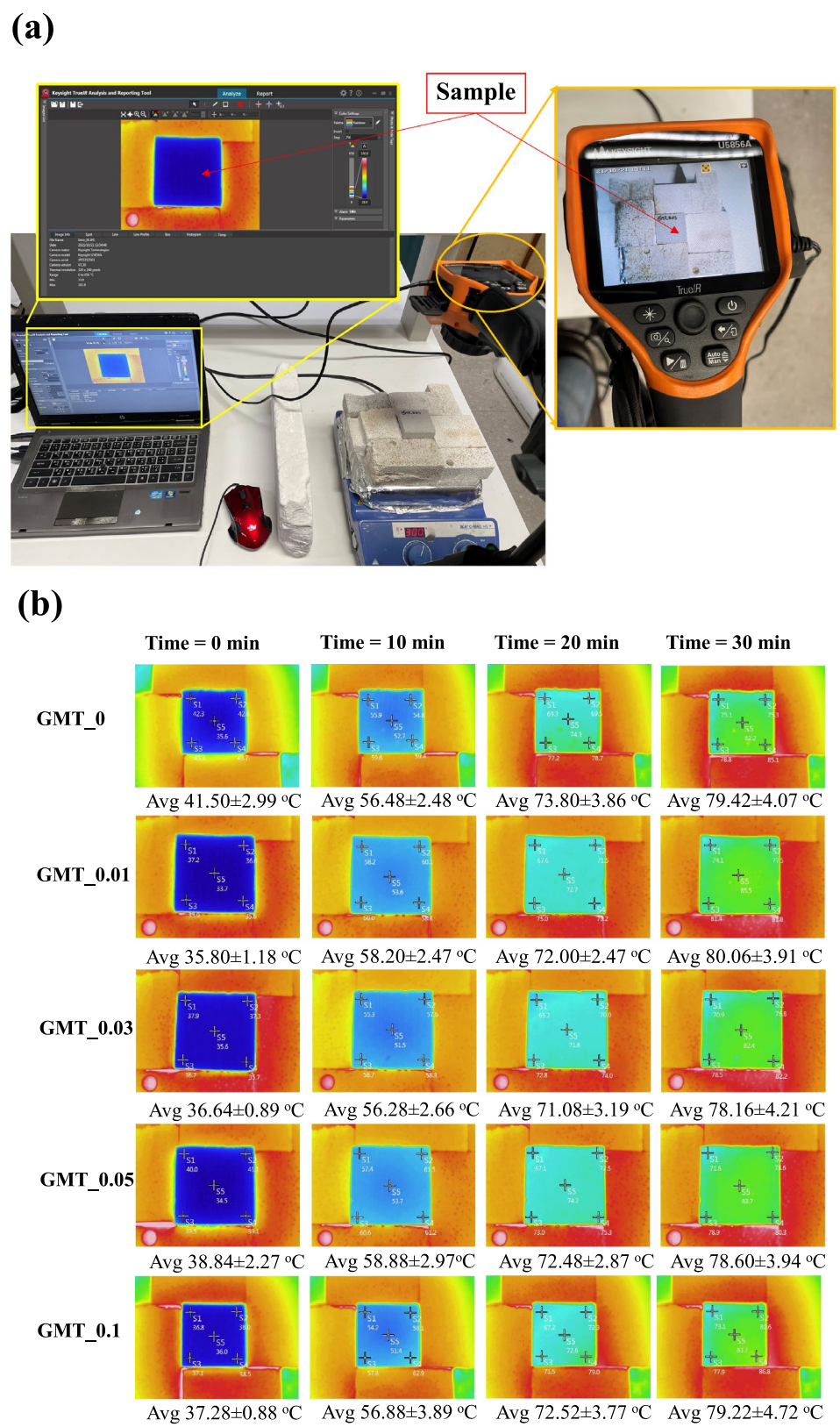

Fig. 7 a The experimantal setup of infrared thermography of the samples. b Infrared thermography images of GMT_0, GMT_0.01, GMT_0.03, GMT_0.05, and GMT_0.1 composites, respectively, at the curing age of 7 days for 0, 10, 20 and 30 min.

Table 3 Thermal conductivity (κ), thermal resistance (*R*), overall heat transfer coefficient (*U*), temperature difference (Δ*T*) and heat transfer rate (*Q*) of GMT_0, GMT_0.01, GMT_0.03, GMT_0.05, and GMT_0.1 composites.

Samples	Thermal conductivity (W/mK)	Thermal resistance (m^2K/W)	Overall heat transfer coefficient (W/m^2K)	Temperature difference (°C)		Heat transfer rate (W/min)	
				20 min	30 min	20 min	30 min
GMT_0	0.577 ± 0.007	0.087	11.556	276.20	270.58	0.793	0.523
GMT_0.01	0.568 ± 0.022	0.088	11.369	278.00	269.94	0.783	0.514
GMT_0.03	0.548 ± 0.025	0.091	10.972	278.92	271.84	0.757	0.498
GMT_0.05	0.512 ± 0.027	0.098	10.252	277.52	271.40	0.705	0.465
GMT_0.1	0.489 ± 0.025	0.102	9.792	277.48	270.78	0.674	0.443

value was 11.556, 11.369, 10.972, 10.252 and 9.792 W/m^2 K for samples of the GMT_0, GMT_0.01, GMT_0.03, GMT_0.05, and GMT_0.1 composites, respectively.

Regarding the heat transfer rate (*Q*), it was calculated by $Q = \kappa A(\Delta T/t)$, where κ is the thermal conductivity of samples; t is the insulation thickness; ΔT is the temperature differences; and, *A* is the arear of sample. The *Q* of GMT composites remained at the cold side for 20 and 30 min. The results demonstrated a decrease in heat transfer rate with increasing GO contents, as displayed in Table 3. These results indicated the effect of GO nanosheet connected with the CSH, CH and CCA phases in the cement mortar on the thermal insulation property of GMT composites (Zhou et al., 2010). The low heat transfer rate of GMT_0.05 and GMT_0.1 composites for 30 min was 0.465 and 0.443 W/min, respectively, indicating lower rate than the samples without GMT_0 composite. Therefore, the GMT composites can be a new pathway to significantly improve the heat insulation of mortar composites.

4 Conclusion

The influence of GO sheets loading contents on the mechanical and thermal properties of the mortar composites was investigated. Three crystalline phases of CaH_2O_4Si, $Ca(OH)_2$, $Ca_6[Al(OH)_6]_2(SO_4)_3{\cdot}26H_2O$ and SiO_2 were observed in all conditions, indicating the mortar material. The size of cement mortar deposited on the surface of GO is slightly decreased with increasing the GO contents. The small particle sizes of mortar, which created the CSH, CH, and CA phases on the surface of GO in the cement mortar, should be explained by increasing the compressive and tensile strength values. Interestingly, the thermal conductivity is decreased with increasing GO contents. The thermal conductivity values of 0.513 ± 0.028 and 0.490 ± 0.026 W/m K for GMT_0.05 and GTO_0.1 composites, respectively, indicate a heat insulator material. Moreover, the low heat transfer rate of GMT_0.05 composite for 30 min was 0.465 W/min, demonstrating a new pathway to significantly improve the heat insulation of mortar composites. The interactions between CSH, CH and CA phases in the cement mortar and GO sheets can affect the heat insulation of GMT composites. Therefore, the mechanical and thermal properties of mortar nanocomposite materials were improved by GO nanosheets.

Acknowledgements
This project is funded by National Research Council of Thailand.

Authors' contributions
JT: data curation, formal analysis, visualization, investigation, writing—original draft. KS: data curation, formal analysis, visualization, investigation, writing—original draft. TW: conceptualization, data curation, formal analysis. KA: data curation, formal analysis, writing—original draft. PC: data curation, formal analysis, writing—original draft. SC: writing—original draft, formal and data analysis. RC: conceptualization, formal analysis, funding acquisition, visualization resources, supervision, validation, writing—original draft, writing—review and editing. All authors read and approved the final manuscript.

Authors' information
Thidatip Janjaroen is a M.Sc. degree student at Department of Applied physics, School of science, King Mongkut's Institute of Technology Ladkrabang, Bangkok, 10520 Thailand, assistant researcher at Smart Materials Research and Innovation Unit, Faculty of Science, King Mongkut's Institute of Technology Ladkrabang, Chalongkrung Road, Ladkrabang, Bangkok, 10520, Thailand, and assistant researcher at Thailand Center of Excellence in Physics, Ministry of Higher Education, Science, Research and Innovation, 328 Si Ayutthaya Road, Bangkok 10400, Thailand.
Sunisar Khammahong is a Ph. D. degree student at Department of Applied physics, School of science, King Mongkut's Institute of Technology Ladkrabang, Bangkok, 10520 Thailand, assistant researcher at Smart Materials Research and Innovation Unit, Faculty of Science, King Mongkut's Institute of Technology Ladkrabang, Chalongkrung Road, Ladkrabang, Bangkok, 10520, Thailand, and assistant researcher at Thailand Center of Excellence in Physics, Ministry of Higher Education, Science, Research and Innovation, 328 Si Ayutthaya Road, Bangkok 10400, Thailand.
Wattana Tuichai is a Post-Doctoral Researcher at school of science, King Mongkut's Institute of Technology Ladkrabang, Bangkok, 10520 Thailand, researcher at Smart Materials Research and Innovation Unit, Faculty of Science, King Mongkut's Institute of Technology Ladkrabang, Chalongkrung Road, Ladkrabang, Bangkok, 10520, Thailand, and researcher at Thailand Center of Excellence in Physics, Ministry of Higher Education, Science, Research and Innovation, 328 Si Ayutthaya Road, Bangkok 10400, Thailand.
Attaphol Karaphun is a Post-Doctoral Researcher at school of science, King Mongkut's Institute of Technology Ladkrabang, Bangkok, 10520 Thailand, researcher at Smart Materials Research and Innovation Unit, Faculty of Science, King Mongkut's Institute of Technology Ladkrabang, Chalongkrung Road, Ladkrabang, Bangkok, 10520, Thailand, and researcher at Thailand Center of

Excellence in Physics, Ministry of Higher Education, Science, Research and Innovation, 328 Si Ayutthaya Road, Bangkok 10400, Thailand.
Chaiwat Phrompet is a Post-Doctoral Researcher at school of science, King Mongkut's Institute of Technology Ladkrabang, Bangkok, 10520 Thailand, researcher at Smart Materials Research and Innovation Unit, Faculty of Science, King Mongkut's Institute of Technology Ladkrabang, Chalongkrung Road, Ladkrabang, Bangkok, 10520, Thailand, and researcher at Thailand Center of Excellence in Physics, Ministry of Higher Education, Science, Research and Innovation, 328 Si Ayutthaya Road, Bangkok 10400, Thailand.
Chaval Sriwong is an Assistant Professor of Inorganic Chemistry at Department of Chemistry, School of Science, King Mongkut's Institute of Technology Ladkrabang, Bangkok, 10520 Thailand, researcher at Smart Materials Research and Innovation Unit, Faculty of Science, King Mongkut's Institute of Technology Ladkrabang, Chalongkrung Road, Ladkrabang, Bangkok, 10520, Thailand, and researcher at Thailand Center of Excellence in Physics, Ministry of Higher Education, Science, Research and Innovation, 328 Si Ayutthaya Road, Bangkok 10400, Thailand.
Chesta Ruttanapun is an Associate Professor of Physics at school of science, King Mongkut's Institute of Technology Ladkrabang, Bangkok, 10520 Thailand, head of Smart Materials Research and Innovation Unit, Faculty of Science, King Mongkut's Institute of Technology Ladkrabang, Chalongkrung Road, Ladkrabang, Bangkok, 10520, Thailand, and researcher at Thailand Center of Excellence in Physics, Ministry of Higher Education, Science, Research and Innovation, 328 Si Ayutthaya Road, Bangkok 10400, Thailand.

Funding
This project is funded by National Research Council of Thailand, Grant Number: 400/2563), Chesta Ruttanapun.

Availability of data and materials
The experimental data were used to support the observations of this study.

Declarations

Ethics approval and consent to participate
Yes.

Consent for publication
The authors declare that they have the consent for publication.

Competing interests
The authors declare that they have no competing interests.

Author details
[1]Smart Materials Research and Innovation Unit, Faculty of Science, King Mongkut's Institute of Technology Ladkrabang, Chalongkrung Road, Ladkrabang, Bangkok 10520, Thailand. [2]Department of Physics, Faculty of Science, King Mongkut's Institute of Technology Ladkrabang, Chalongkrung Road, Ladkrabang, Bangkok 10520, Thailand. [3]Thailand Center of Excellence in Physics, Ministry of Higher Education, Science, Research and Innovation, 328 Si Ayutthaya Road, Bangkok 10400, Thailand. [4]Department of Chemistry, Faculty of Science, King Mongkut's Institute of Technology Ladkrabang, Chalongkrung Road, Ladkrabang, Bangkok 10520, Thailand.

Received: 10 December 2021 Accepted: 21 March 2022
Published online: 07 July 2022

References

Bo, L. (2005). Technology research on oxidative degree of graphite oxide prepared by hummers method. *Carbon, 4*, 10–14.
Cao, M., Zhang, C., & Wei, J. (2013). Microscopic reinforcement for cement based composite materials. *Construction and Building Materials, 40*, 14–25.
Carrasco, M., Del Campo, A., Rubia, M. A., Reyes, E., Moragues, A., & Fernández, J. (2017). New insights in weathering analysis of anhydrous cements by using high spectral and spatial resolution Confocal Raman Microscopy. *Cement and Concrete Research, 100*, 119–128.
Compton, O. C., & Nguyen, S. T. (2010). Graphene oxide, highly reduced graphene oxide, and graphene: Versatile building blocks for carbon-based materials. *Small (weinheim an Der Bergstrasse, Germany), 6*(6), 711–723.
De Jong, K. P., & Geus, J. W. (2000). Carbon nanofibers: Catalytic synthesis and applications. *Catalysis Reviews, 42*(4), 481–510.
De Volder, M. F. L., Tawfick, S. H., Baughman, R. H., & Hart, A. J. (2013). Carbon nanotubes: Present and future commercial applications. *Science, 339*(6119), 535–539.
Dissanayake, D. M. K. W., Jayasinghe, C., & Jayasinghe, M. T. R. (2017). A comparative embodied energy analysis of a house with recycled expanded polystyrene (EPS) based foam concrete wall panels. *Energy and Buildings, 135*, 85–94.
Du, M., Jing, H., Gao, Y., Su, H., & Fang, H. (2020). Carbon nanomaterials enhanced cement-based composites: Advances and challenges. *Nanotechnology Reviews, 9*, 115–135.
Ferrándiz-Mas, V., Bond, T., García-Alcocel, E., & Cheeseman, C. R. (2014). Lightweight mortars containing expanded polystyrene and paper sludge ash. *Construction and Building Materials, 61*, 285–292.
Geim, A. K., & Novoselov, K. S. (2007). The rise of graphene. *Nature Materials, 6*(3), 183–191.
Gholampour, A., Kiamahalleh, M. V., Tran, D. N. H., Ozbakkaloglu, T., & Losic, D. (2017). From graphene oxide to reduced graphene oxide: impact on the physiochemical and mechanical properties of graphene-cement composites. *ACS Applied Materials & Interfaces, 9*(49), 43275–43286.
Goracci, G., & Dolado, J. S. (2020). Elucidation of conduction mechanism in graphene nanoplatelets (GNPs)/cement composite using dielectric spectroscopy. *Materials, 13*(2), 275.
Jiang, D., An, P., Cui, S., Xu, F., Tuo, T., Zhang, J., & Jiang, H. (2018). Effect of leaf fiber modification methods on mechanical and heat-insulating properties of leaf fiber cement-based composite materials. *Journal of Building Engineering, 19*, 573–583.
Kang, D., Seo, K. S., Lee, H., & Chung, W. (2017). Experimental study on mechanical strength of GO-cement composites. *Construction and Building Materials., 131*, 303–308.
Kaya, A., & Kar, F. (2016). Properties of concrete containing waste expanded polystyrene and natural resin. *Construction and Building Materials, 105*, 572–578.
Kim, J., Cote, L. J., Kim, F., Yuan, W., Shull, K. R., & Huang, J. (2010). Graphene oxide sheets at interfaces. *Journal of the American Chemical Society, 132*(23), 8180–8186.
Li, J., Xiang, Q., Ze, R., Ma, M., Wang, S., Xie, Q., & Xiang, Y. (2018). Thermal and electrical analysis of SiGe thermoelectric unicouple filled with thermal insulation materials. *Applied Thermal Engineering, 134*, 266–274.
Li, V. C., & Leung, C. K. Y. (1992). Steady-state and multiple cracking of short random fiber composites. *Journal of Engineering Mechanics, 118*(11), 2246–2264.
Liu, L., Zhang, J., Zhao, J., & Liu, F. (2012). Mechanical properties of graphene oxides. *Nanoscale, 4*(19), 5910–5916.
Liu, Y., Wang, F., Liu, M., & Hu, S. (2014). A microstructural approach to adherence mechanism of cement and asphalt mortar (CA mortar) to repair materials. *Construction and Building Materials, 66*, 125–131.
Llobet, E. (2013). Gas sensors using carbon nanomaterials: A review. *Sensors and Actuators b: Chemical, 179*, 32–45.
Lojka, M., Lauermannová, A.-M., Sedmidubský, D., Pavlíková, M., Záleská, M., Pavlík, Z., Pivák, A., & Jankovský, O. (2021). Magnesium oxychloride cement composites with MWCNT for the construction applications. *Materials, 14*(3), 484.
Lv, S., Liu, M., He, W., Li, X., Gong, W., & Shen, S. (2020). Study of thermal insulation materials influence on the performance of thermoelectric generators by creating a significant effective temperature difference. *Energy Conversion and Management, 207*, 112516.
Lv, S., Ma, Y., Qiu, C., Sun, T., Liu, J., & Zhou, Q. (2013). Effect of graphene oxide nanosheets of microstructure and mechanical properties of cement composites. *Construction and Building Materials, 49*, 121–127.
Mahanta, N.; Abramson, A. Thermal conductivity of graphene and graphene oxide nanoplatelets. 13th InterSociety Conference on Thermal and Thermomechanical Phenomena in Electronic Systems 2012.
Marcano, D. C., Kosynkin, D. V., Berlin, J. M., Sinitskii, A., Sun, Z., Slesarev, A., Alemany, L. B., Lu, W., & Tour, J. M. (2010). Improved synthesis of graphene oxide. *ACS Nano, 4*(8), 4806–4814.

Naganathan, S., Singh, C. S. J., Shen, Y. W., Kiat, P. E., & Thiruchelvam, S. (2014). Nanotechnology in civil engineering—A review. *Advanced Materials Research, 935*, 151–154.
Namsone, E.; Sahmenko, G.; Namsone, E.; Korjakins, A. Thermal conductivity and frost resistance of foamed concrete with porous aggregate, Environment. Technology. Resources. In: Proceedings of the 11th International Scientific and Practical Conference, Rezekne, Latvia, 15–17 June 2017; Volume 3, pp. 222–228.
Phrompet, C., Sriwong, C., & Ruttanapun, C. (2019). Mechanical, dielectric, thermal and antibacterial properties of reduced graphene oxide (rGO)-nanosized C3AH6 cement nanocomposites for smart cement-based materials. *Composites Part B Engineering, 175*, 107128.
Popov, V. N. (2004). Carbon nanotubes: Properties and application. *Materials Science and Engineering: r: Reports, 43*(3), 61–102.
Qian, Y.; Abdallah, M.Y.; Kawashima, S. (2015). of cement-based materials modified with graphene-oxide. *Nanotechnology in Construction,* 259–264.
Qureshi, T. S., & Panesar, D. K. (2019). Impact of graphene oxide and highly reduced graphene oxide on cement based composites. *Construction and Building Materials, 206*, 71–83.
Rafiee, M. A., Narayanana, T. N., Hashim, D. P., Sakhavand, N., Shahsavari, R., Vajtai, R., & Ajayan, R. M. (2013). Hexagonal boron nitride and graphite oxide reinforced multifunctional porous cement composites. *Advanced Functional Materials, 23*(45), 5624–5630.
Raki, L., Beaudoin, J., Alizadeh, R., Makar, J., & Sato, T. (2010). Cement and concrete nanoscience and nanotechnology. *Materials, 3*(2), 918–942.
Roychand, R., De Silva, S., Law, D., & Setunge, S. (2016). High volume fly ash cement composite modified with nano silica, hydrated lime and set accelerator. *Materials and Structures, 49*(5), 1997–2008.
Sagar, R. V., Prasad, B. K. R., & Kumar, S. S. (2012). An experimental study on cracking evolution in concrete and cement mortar by the b-value analysis of acoustic emission technique. *Cement and Concrete Research, 42*(8), 1094–1104.
Sanchez, F., & Sobolev, K. (2010). Nanotechnology in concrete—A review. *Construction and Building Materials, 24*(11), 2060–2071.
Singh, L. P., Goel, A., Bhattachharyya, S. K., Ahalawat, S., Sharma, U., & Mishra, G. (2015). Effect of morphology and dispersibility of silica nanoparticles on the mechanical behaviour of cement mortar. *International Journal of Concrete Structures and Materials, 9*(2), 207–217.
Suk, J. W., Piner, R. D., An, J., & Ruoff, R. S. (2010). Mechanical properties of monolayer graphene oxide. *ACS Nano, 4*(11), 6557–6564.
Wang, L., Wang, J., Qian, X., Chen, P., Xu, Y., & Guo, J. (2017). An environmentally friendly method to improve the quality of recycled concrete aggregates. *Construction and Building Materials, 144*, 432–441.
Wang, W., Sha, A., Lu, Z., Jia, M., Jiang, W., Liu, Z., & Yuan, D. (2021). Self-luminescent cement-based composite materials: properties and mechanisms. *Construction and Building Materials, 269*, 121267.
Xu, Z., & Gao, C. (2011). Aqueous liquid crystals of graphene oxide. *ACS Nano, 5*(4), 2908–2915.
Yang, Y., Cao, J., Wei, N., Meng, D., Wang, L., Ren, G., Yan, R., & Zhang, N. (2019). Thermal conductivity of defective graphene oxide: A molecular dynamic study. *Molecules, 24*(6), 1103.
Yousefi, A., Tang, W., Khavarian, M., Fang, C., & Wang, S. (2020). Thermal and mechanical properties of cement mortar composite containing recycled expanded glass aggregate and nano titanium dioxide. *Applied Sciences, 10*, 2246.
Zhou, X.-Y., Zheng, F., Li, H.-G., & Lu, C.-L. (2010). An environment-friendly thermal insulation material from cotton stalk fibers. *Energy and Buildings, 42*(7), 1070–1074.
Zhou, Y., He, J., Wang, H., Qi, K., Ding, B., & Cui, S. (2016). Carbon nanofiber yarns fabricated from co-electrospun nanofibers. *Materials & Design, 95*, 591–598.
Zhu, Y., Murali, S., Cai, W., Li, X., Suk, J. W., Potts, J. R., & Ruoff, R. S. (2010). Graphene and graphene oxide: Synthesis, properties, and applications. *Advanced Materials, 22*(35), 3906–3924.

Publisher's Note